Emission Lines in Active Galaxies: New Methods and Techniques
ASP Conference Series, Vol. 113, 1997
B.M. Peterson, F.-Z. Cheng, and A.S. Wilson (eds.)

Coronal Lines in Active Galactic Nuclei

E. Oliva
Osservatorio Astrofisico di Arcetri, Largo E. Fermi 5, I-50125 Firenze, Italy

Abstract. Recent observations show that the CLR[1] is small (a few tens of parsecs), has large column densities ($N \approx 10^{22}\,\mathrm{cm}^{-2}$), and lies close to and is probably photoionized by the AGN. Coronal lines give information on Ne, Mg, Si, S, Ca, and Fe abundances, on the dust content and dynamics of the CLR, and can be used to trace hidden AGN. If they are powered by photoionization, coronal lines could be used to reconstruct the AGN spectrum at 100–400 eV. However, a proper understanding of the results requires careful use of photoionization codes, since the ionization parameter at the inner face is probably meaningless for CLR models, and a reliable convergence of the 'highly variable' atomic parameters for coronal lines. A shock model for the CLR in NGC 1068 requires collisional ionization of $\geq 600\,M_\odot\,\mathrm{yr}^{-1}$ of dense ($n > 10^4\,\mathrm{cm}^{-3}$) gas within a region no larger than 30 pc. Maintaining a shock-excited CLR for a reasonable time requires $> 10^{10}\,M_\odot$ of fuel, which must be continuously supplied to the CLR.

1. Introduction

Coronal lines are forbidden transitions within low-lying levels which, like [O III] and other forbidden lines, are excited by collisions. Their only peculiarity is the high ionization of the emitting species (≥ 100 eV); the misleading label *coronal* is only used because they were first observed in the solar corona. The origin of coronal ions is a debated issue which so far has attracted most of the attention of observers and theoreticians. In photoionization models, the CLR is powered by the soft X-rays (100–400 eV) from the AGN (e.g., Grandi 1978 [hereafter G78], Korista & Ferland 1989). In collisionally ionized models, the energy input is by fast shocks that heat the gas to $\geq 10^6$ K (e.g., Viegas-Aldrovandi & Contini 1989 [VC89]).

Observationally, optical AGN spectra often show the well-known iron coronal lines ([Fe VII], [Fe X], [Fe XI],) some of which were already identified in the original work of Seyfert (1943). The lines are strong, 1–20% the strength of Hβ, and their profiles are systematically blueshifted relative to lower excitation species ([G78], Penston et al. 1984 [P84]). A similar blueshift was also

[1]The coronal-line region (CLR) is defined as the region producing [Fe X, XI], [S VIII, IX] and [Si IX, X].

found in the IR lines (Oliva et al. 1994 [O94], Marconi et al. 1996 [Ma96]). Coronal lines are often broader than, for example, [O III] but little is known above $h\nu_{ion} > 100\,\mathrm{eV}$ (i.e., beyond [Fe VII] and [Ne V]). A remarkable exception is NGC 1068, where [Fe XI] and [Si IX] are significantly narrower than [Fe VII] (Ma96). Interest in coronal lines was recently revived by observations at longer wavelengths starting with the detection of [S VIII] λ9913 (Osterbrock et al. 1990) and [Si VI] $\lambda 1.963\,\mu$m (Oliva & Moorwood 1990), followed by detection of [Si VII], [Si IX], [S IX], [Ca VIII] (O94, Ma96), [Si X] (Thompson 1996), and [Al IX] (Maiolino et al. 1997), and *ISO* observations of [Ne V], [Ne VI], [Mg V], [Mg VII], and [Mg VIII] (Moorwood et al. 1996 [Mo96]).

2. Observed Parameters and Simple Interpretation

Table 1 is a list of parameters for two nearby Seyferts and template objects. The most striking feature is the small size and large surface brightness of the CLR.

Table 1. Observed Properties of Coronal Lines

	Circinus [a]	NGC 1068 [b]	LMC–N49 [c]	NGC 6302 [d]
L([Fe XI]) (ergs s^{-1})	2×10^{38}	4×10^{39}	3×10^{34}	$< 10^{30}$
L([Si VI]) (ergs s^{-1})	3×10^{38}	3×10^{40}	...	4×10^{33}
Diameter (pc) [e]	≤ 12	≤ 28	19	0.05
Σ([Fe X, XI]) [f]	$\geq 10^{-2}$	$\geq 3 \times 10^{-2}$	7×10^{-6}	$< 3 \times 10^{-6}$
Σ([Si VI]) [f,g]	$\sim 5 \times 10^{-3}$	$\sim 10^{-2}$	$< 4 \times 10^{-5}$	1.3×10^{-2}
[Fe XI]/Hβ	0.10	0.07 [h]	0.01	$< 10^{-3}$
[Fe XI]/[Fe II] λ8617	> 3	> 2	0.1	...
[Fe XI]/[O I] λ6300	0.18	0.11	0.01	$< 5 \times 10^{-3}$
[S VIII]/[Fe X]	0.42	1.1	...	> 30
[Si IX]/[Si VI]	2.1	0.63	...	$< 2 \times 10^{-3}$
FWHM [i] (km s^{-1})	< 150	950	...	< 200

[a] Seyfert 2, data from O94, assumed distance $D = 4$ Mpc.

[b] Data from Ma96, D=19 Mpc, size and Σ([Fe X]) from archive *HST* data.

[c] A powerful SNR, data from Russel & Dopita (1990) and unpublished IRSPEC spectra, $D = 52$ kpc.

[d] The highest excitation PN, data from Ashley & Hyland (1988), Reconditi & Oliva (1993) and Ma96, $D = 1$ kpc.

[e] For AGN size of the [Fe X] region, [Fe VII] and [Si VI] are more extended.

[f] Surface brightness, ergs s^{-1} cm^{-2} sr^{-1}.

[g] Σ[Si VI] from 3D data.

[h] In NGC 1068, the ratio [Fe X]/Hβ in a 0$''$.3 aperture is 0.25.

[i] Width of [Fe XI] in AGNs, width of [Si VI] in NGC6302.

2.1. Column and Gas Densities

The column density and gas density of the CLR are related to the line surface brightness Σ by

$$N n_e = \frac{4\pi\Sigma}{(n(X^{+i})/n_e)j} \ \mathrm{cm}^{-5} \tag{1}$$

and

$$n_e = \left(\frac{4\pi\Sigma}{(n(X^{+i})/n_e)j\theta D f}\right)^{1/2} \ \mathrm{cm}^{-3} \tag{2}$$

where N is the column density, n_e is the mean electron density, $n(X^{+i})$ is the number density of the emitting species, j (ergs s^{-1} cm^3) is the line emission coefficient, θD is the projected size of the CLR and f is its filling factor. In eq. (2), it is assumed that the emitting region is spherically symmetric. Typical values for [Fe XI] are $\Sigma \geq 0.01$ (Table 1), $j \approx 10^{-20}$ (Fig. 2, below), and $n_X/n_e \approx 10^{-5}$, which yields $n_e \approx 300 f^{-1/2}\,\mathrm{cm}^{-3}$ and $N \approx 10^{22} f^{1/2}\,\mathrm{cm}^{-2}$, i.e., a column density only a factor of 10 lower than those found in warm absorbers (Netzer 1997). Direct measurement of n_e is also possible using density-sensitive line ratios such as [Ne V] λ14.3 μm/[Ne V] λ24.3 μm, since both lines are now accessible with *ISO*. In the Circinus galaxy, this yields $n_e \approx 5000\,\mathrm{cm}^{-3}$ (Mo96) which, apart for the possible uncertainties on the atomic parameters discussed below, indicates that the CLR could be even smaller than 12 pc (=0$''$.6, O94) and/or have a small filling factor.

2.2. Comparison with Shock-Excited Templates (SNRs)

The supernova remnant (SNR) LMC–N49 is the most luminous line source among Galactic and LMC/SMC remnants and therefore a good prototype of shocks that are strongly interacting with the interstellar medium. The AGN CLRs have roughly the same size as the SNRs, but are 4–5 orders of magnitude more luminous or, equivalently, have a surface brightness a factor 10^{4-5} higher (cf. Table 1). This clearly indicates that powering the CLR with shocks requires extreme conditions, effectively very high pre-shock densities (cf. §4).

The [Fe XI]/Hβ ratio in SNRs is typically an order of magnitude lower than in AGN, but photoionization contributes to (and probably dominates) the production of Hβ in Seyferts. A shock-excited CLR should therefore be characterized by a [Fe XI]/Hβ ratio close to unity and a factor ≥ 100 larger than in SNRs. The ratio [Fe XI]/[Fe II] λ8617 is also of interest because in shocks it measures the relative column densities of the hot material immediately after the shock and of the cooler recombination region farther behind. [Fe II]λ8617 is not detected in Seyferts, while it is 10 times brighter than [Fe XI] in N49 and other SNRs. The same is found using other bright low-ionization lines with high critical densities ($n_c > 10^6\,\mathrm{cm}^{-3}$) such as [O I] (Table 1), [Ca II] λ7291 and [Ni II] λ7380.

These results imply that the shocked material should not recombine on a time scale comparable to the age of the CLR, and this is hard to account for given the high pre-shock densities (§4). Alternatively, the recombination zone could be much denser than the critical density of the low-ionization lines, i.e., $n_e > 10^7\,\mathrm{cm}^{-3}$, and not far from those typical of broad-line regions, but this does not help explain the large [Fe XI]/Hβ ratio.

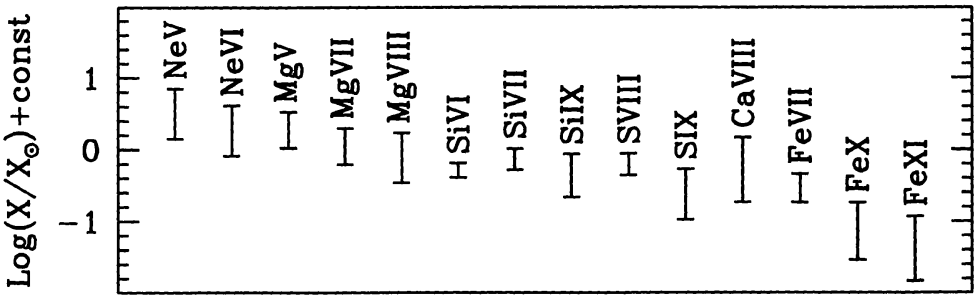

Figure 1. Relative abundances of coronal species in the Circinus galaxy.

A result which is incompatible with emission from collisionally ionized shocked gas are the narrow lines of the Circinus galaxy which have widths (FWHM) less than $150\,\mathrm{km\,s^{-1}}$ (O94), well below the $300\,\mathrm{km\,s^{-1}}$ minimum shock velocity required to collisionally ionize Fe^{+10} (VC89). Narrow lines are also found in NGC 4507 where FWHM([Si VI]) $\leq 200\,\mathrm{km\,s^{-1}}$ (Marconi et al. 1994 [M94]).

2.3. Comparison with Photoionized Templates (PNs)

NGC 6302 is a high-excitation planetary nebula (PN) that hosts one of the hottest stars known, $T_* \approx 250{,}000\,\mathrm{K}$ (Ma96). It is a powerful source of [Si VI, VII], with surface brightness close to those of AGN. This indicates that the CLR could be a scaled-up version of the PN with a much more luminous central source. The ionizing spectrum of the AGN must be harder, however; this is most clearly demonstrated by the [Si IX]/[Si VI] ratio, which is of order unity in AGN and $< 2 \times 10^{-3}$ in PNs. This reflects the fact that a blackbody-like stellar spectrum dramatically drops beyond 200 eV, while the AGN continuum remains quite flat. This simple result indicates that peculiarly hot stars (Terlevich's 'warmers') cannot account for the observed properties of the CLR.

A puzzling feature of NGC 6302 is that all the iron lines are very faint, including [Fe VII], which is only barely detected (Oliva et al. 1996 [O96]) and which should have an intensity similar to [Si VI] (M94). Translated into element abundances, this implies that iron is depleted by a factor of 10^3, i.e., iron is still locked into grains, while silicon is mostly in the gas phase. This probably means that Fe-based grains can survive the very strong stellar radiation field. The Fe abundance and dust content of the CLR are not therefore trivial arguments.

2.4. Element Abundances and Dust Content

Regardless of the ionization mechanism, the relative intensities of coronal lines can be directly related to the abundances of the emitting species. Under the very reasonable assumption that all the lines are below their critical densities (e.g., $3{\times}10^7$, 3×10^8, and $10^9\,\mathrm{cm^{-3}}$ for [Fe VII], [Si VI], and [Fe X, XI], respectively), the line fluxes are simply proportional to the abundances times the emission coefficient j.

The resulting abundances, based on the ground-based data of O94 and on the *ISO*-SWS spectra of Mo96, are plotted in Fig. 1, where the error bars reflect only the uncertainties in atomic parameters, which sometimes exceed 1 dex (O96

and §5). Apart from the curious trend of decreasing abundance with increasing atomic weight, Fig. 1 shows that refractory species (Mg, Si, Ca, and Fe) are not significantly depleted relative to S, and this implies that the CLR is much less dusty than the typical ISM, where Ca and Fe are depleted by 2–3 orders of magnitude. A similar conclusion holds for NGC 1068 (Ma96) and other Seyferts in which the observed [S VIII]/[Fe X, XI] ratios are close to unity. Information on absolute abundances (relative to H) requires proper modeling to correct for the relative volumes of CLR and H II regions. Results of a toy model for Circinus indicate that heavy-element abundances are not far from solar values (Mo96).

2.5. Dynamics of the CLR

Optical coronal lines are systematically blueshifted relative to lower-excitation species (G78, P84), and the same blueshifts are also seen in IR lines (O94, Ma96). A simple explanation follows from the fact that the CLR is close to the nucleus. If material flowing out from the AGN is responsible for the blueshifted components, these are stronger in coronal lines because they form in regions where the dynamical effect of the AGN dominates over larger-scale motions (e.g., galactic rotation) which are more evident in lower-excitation lines that form farther out. This simple model agrees with detailed dynamical studies of NGC 1068 (Ma96). Somewhat puzzling is that the IR lines do not show any obvious extra emission extending to the red. In a bipolar outflow, the redshifted component should become visible at long enough wavelengths. As this is not seen even in [Si IX] $\lambda 3.395\,\mu$m, this either implies that the outflow is asymmetric or that the red component is absorbed by at least $A_V \approx 30$ mag, an optical depth still within the range of molecular clouds. Any conclusion on the role of the torus in obscuring the counter-cone (if any) is therefore premature.

3. Photoionization Models

The main coolant of a photoionized CLR is O VI $\lambda\lambda 1035$, which keeps electrons at $T_e \approx 2$–4×10^4 K, temperatures where the collision strengths (Υ) may vary by more than 1 dex depending on the treatment of resonances (O96). As line fluxes are directly proportional to Υ, predictions should be taken with some care, especially when using results from codes or tables without knowing which values of Υ are used.

Much care should also be taken in using the ionization parameter at the inner face of the cloud, $U_{in} = Q/4\pi r_{in}^2 nc$. In a plane-parallel geometry, U_{in} uniquely defines the structure of a cloud photoionized by a source with a given spectral shape, and the choice of the total ionizing rate Q and gas density n has no influence as long as Q/n is constant and n is below the critical density of the main coolants and of the lines of interest. As the CLR lies very close to the AGN (probably $r < 1$ pc) and extends over $\Delta R \approx 10$ pc, it is therefore a quasi-spherically symmetric region where the value of U_{in} is meaningless, while a proper 'ionization parameter' is the value of U at the radius of the Strömgren sphere, which scales as

$$U(\text{Strömgren}) \propto Q^{1/3} n^{1/3} f^{2/3}. \qquad (3)$$

The most curious result is that the ionization degree *increases* with n and the choice of the filling factor f has dramatic effects on the ionization structure of a spherical nebula, while f has no influence in plane-parallel models. More details on this subject can be found in §4 of M94, where U(Strömgren) was improperly called Ξ (our apologies to J. Krolik).

4. Collisional Ionization and Shock Models

The most direct test for collisional ionization is the strength of temperature–sensitive line ratios which requires access to lines from levels with $E/k \geq 10^5$ K and which lie close to or beyond the Lyman limit. Interesting diagnostics are listed in Table 2. The UV lines practically disappear at 3×10^4 K, and remain quite weak even at coronal temperatures. Also, the somewhat brighter [Si VII] λ1049 may be blended with the prominent O VI $\lambda\lambda$1032, 1038.

Table 2. Temperature-Sensitive Line Ratios [a]

Ratio:	[Si VII] λ1049/λ2.483 μm		[Si IX] λ950/λ3.395 μm		[Fe XI] λ1467/λ7892	
$\log T$:	3.5	5.8	3.5	6.0	3.5	6.0
	0.045	1.05	0.015	0.52	0.006	0.022
	(0.032)	(0.86)	(0.004)	(0.35)	(0.003)	(0.037)

[a]Values in parentheses are from resonance-dominated Υ (ground state).

At the temperatures required to collisionally ionize the CLR ($0.5–2 \times 10^6$ K), the gas cools very rapidly and could be thermally unstable. It is therefore reasonable to assume that the material freely cools after being heated by the shock, i.e., that there is a steady cooling flow behind the shock front. Under these conditions the total luminosity of a given line is simply proportional to $\dot{M}$, the rate at which mass is processed by the shock. Using the formalism of Graney & Sarazin (1990 [GS90]), the luminosity of a given line L_λ can be expressed as

$$L_\lambda = \Gamma_\lambda \dot{M} \quad ; \quad \Gamma_\lambda = \frac{5k}{2\mu m_p} \int_{T_l}^{T_u} \frac{\Lambda_\lambda(T)}{\Lambda(T)} dT \quad ; \quad \Lambda_\lambda(T) = \frac{n(X^{+i})}{n(X)} \frac{n(X)}{n_p} j \qquad (4)$$

where $\Lambda(T)$ (ergs s^{-1} cm^3) is the total gas cooling, while $\Lambda_\lambda(T)$ is the cooling due to the line. The gas is in ionization equilibrium if recombinations are faster than collisional ionizations, as happens below 10^6 K, where most of the ions of interest are formed (VC89, GS90). Under equilibrium conditions, the ionization fraction $n(X^{+i})/n(X)$ is a known function of T and Γ_λ can be computed as described in GS90. The values in Table 3 are for $T_u > 4 \times 10^6$ K and solar abundances; lower metallicities give similar results if the relative metal abundances are kept constant (GS90). The values of Γ_λ are relatively insensitive to the chosen collision strengths because the lines are mostly produced by indirect collisions to high-energy states where the values of Υs are little influenced by resonances (Fig.

2). The large [Fe XIV]/[Fe X] ratio of Table 3 increases further if non-equilibrium ionization is considered; this delays the recombination of Fe^{+13} and produces stronger [Fe XIV] (GS90). Collisionally ionized regions are therefore characterized by large [Fe XIV]/[Fe X] ratios, and the lower (< 1) values found in AGN can be explained only by introducing a temperature cutoff at $T_u \approx 1.5 \times 10^6$ K, a result that was already found by Nussbaumer & Osterbrock (1970).

Table 3. Line Emission by Cooling Gas[a]

Line	Γ_λ		Line	Γ_λ	
[Fe X] λ6374	6.7	(10)	[Fe XI] λ7892	9.2	(22)
[Fe XIV] λ5303	32	(42)[b]	[Si VI] $\lambda 1.963\,\mu$m	0.91	(1.3)
[Si VII] $\lambda 2.483\,\mu$m	1.4	(1.7)	[Si IX] $\lambda 3.395\,\mu$m	2.6	(3.1)
[S VIII] λ9913	0.76	(0.98)	[S IX] $\lambda 1.252\,\mu$m	1.1	(1.8)
[Si X] $\lambda 1.43\,\mu$m	4.3	(5.6)			

[a] Γ_λ in units of 10^{10} ergs g^{-1}, values in parentheses are derived using resonance-dominated Υ values for the ground-state levels, cf. §5.

[b] Values reduce to 4.3 (6.2) if $T_u = 1.6 \times 10^6$ K (cf. eq. 4).

The density of the pre-shock gas is related to the line surface brightness by

$$4\pi\Sigma = \Gamma_\lambda \rho_o v_s \quad ; \quad \Sigma([\mathrm{Fe\,X, XI}]) \approx 5 \times 10^{-7} n_0 \left(\frac{v_s}{200\,\mathrm{km/s}}\right) \ \mathrm{erg\,cm^{-2}\,s^{-1}\,sr^{-1}} \tag{5}$$

and must be $n_0 \geq 2 \times 10^4$ to account for the observed values of Σ (cf. Table 1). The mass cooling rate required to produce the observed line luminosities can be estimated from eq. (4) (left), which yields 30 and 600 $M_\odot\,\mathrm{yr}^{-1}$ for Circinus and NGC 1068, respectively. The *total* (gas+stars) virial mass in the central 100 pc inferred from stellar velocity dispersions ($\sim 165\,\mathrm{km\,s^{-1}}$ for both galaxies, Oliva et al. 1995) is $6 \times 10^8\,M_\odot$, so there is far too little gas to feed the shock for a reasonable time ($> 10^7$ yr). A shock-heated CLR should therefore be continuously fed with dense gas (molecular clouds?) from the galaxy, and the total amount of fuel needed is huge, more than 10^9 and more than $10^{10}\,M_\odot$ in Circinus and NGC 1068, respectively.

5. Atomic Parameters and Collision Strengths

All atomic parameters for coronal ions are quite uncertain, but ionization cross-sections and recombination coefficients only define *where and when* coronal species are formed. Errors on these parameters affect the ionization structure and conclusions drawn from photoionization or collisional-ionization models. Collision strengths (Υ) define *how strong* the coronal lines are, and errors on

Υ have direct consequences on even the simplest interpretation of observed line fluxes.

Free electrons can collisionally excite an ion X_l^{+i} to a state u through normal Coulomb interaction or via radiationless transitions to or from a doubly excited state of X^{+i-1} lying above its ionization threshold

$$X_l^{+i} + e^-(E) \rightarrow X_*^{+i-1} \rightarrow X_u^{+i} + e^-(E - \Delta E), \quad (6)$$

where E is the kinetic energy of the electron and $\Delta E = E_u - E_l$. For the resonance to work, the free e^- must have the same energy of the autoionizing state X_*^{+i-1} and the quantum numbers of the states involved must fulfill the selection rules for radiationless transitions (Herzberg 1944). The process is therefore a close relative of the much slower dielectronic recombinations

$$X_l^{+i} + e^-(E) \rightarrow X_*^{+i-1} \rightarrow X^{+i-1} + h\nu,$$

where the autoionizing level radiatively decays to a 'true bound state' X^{+i-1} (a very clear description of this process can be found in Bates & Dalgarno 1962). Resonant excitations as in eq. (6) are very fast and produce prominent peaks ('resonances') in the cross-sections, whose widths are mainly related to the number of autoionizing levels available for the process. The number of resonances can be large in coronal lines because the selection rules mentioned above are particularly lax for ground state $\Delta J = \pm 1$, $\Delta S, \Delta L = 0$ transitions, and computed cross-sections often show groups of resonances much broader than 10^3 K. At the temperatures typical of photoionized gas ($2\text{–}4 \times 10^4$ K), collision rates dramatically depend on where these resonances are, and the Maxwellian-averaged collision strength Υ may increase by large factors if the autoionizing levels lie just above the ground state of X^{+i}. The major problem is that the position of these unobserved autoionizing levels is quite uncertain because extrapolated from known bound states whose energies are often known with errors $> 10^4$ K, and in some coronal ions not even the ionization limit is accurately known. Changing the positions of the resonances by only a few thousand degrees may have dramatic effects on the computed value of Υ at $2\text{–}4 \times 10^4$ K, and this possible uncertainty is usually not mentioned; remarkable exceptions are Saraph & Tully (1994 [ST94]), Galavis et al. (1995), and Saraph & Storey (1996).

The effect of resonances at $T = 2\text{–}4 \times 10^4$ K is evident in Fig. 2, which plots the line emission coefficient j (ergs s^{-1} cm^{-3}) defined so that the line luminosity from a given volume V of gas is $L = N(X^i)N_e jV$ ergs s^{-1}.

The current status for some of the lines of interest is as follows:

- [Ne V] $\lambda\lambda$14.3, 24.3 μm: Old *IRAS*+*KAO* data for PNs indicate that Υ's were overestimated (O96), but new *ISO*-SWS spectra give different line fluxes which seem in better agreement with computed values of Υ (Mo96).

- [Si VI] λ1.963 μm & [S VIII] λ9913: Resonances seem to have small effects, as values of Υ by ST94 are only a factor < 1.5 above the old values of the Kafatos & Lynch (1980 [KL80]) and Mendoza (1983) compilations.

- [Ne VI] λ7.65 μm, [Mg VIII] λ3.027 μm, & [Si X] λ1.43 μm: Resonances are strong and Υ's from Zhang et al. (1994) are factors 5–9 larger than in

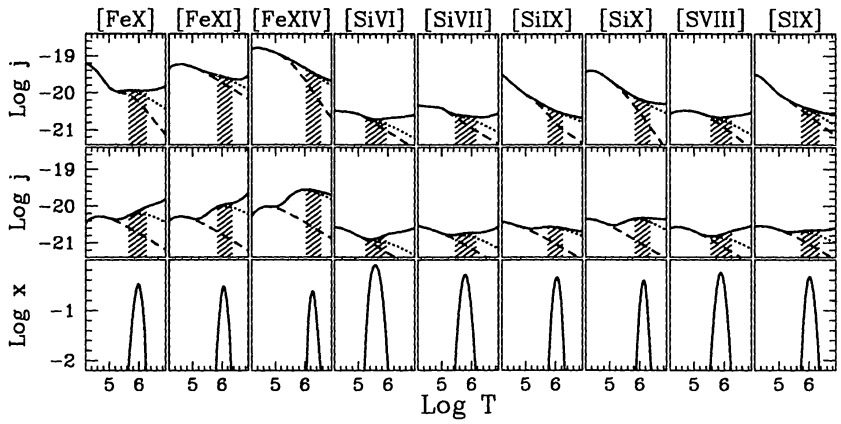

Figure 2. Ionization fraction x for collisional equilibrium. Line emission coefficient j including (top) and neglecting resonances in Υ. Dashed lines: only direct e^- collisions, dotted: with collisions to high-lying states, solid: with proton collisions (cf. O94, Ma96).

KL80 and M93. Note that the values in the printed tables of Zhang et al. differ from those in the electronic files available at CDS.[2]

- [Si VII] λ2.483 μm & [S IX] λ1.252 μm: Collision strengths of Butler & Zeippen (1994) are 2 and 9 times larger than those of KL80, respectively.
- [Ca VIII] λ2.321 μm: Saraph & Storey (1996) find broad resonances which increase Υ by a factor of 9.
- [Fe X] λ6374, [Fe XI] λ7892, & [Fe XIV] λ5303: Resonances produce factors of >10 increase in Υ which were already estimated (and labeled Ω^{eff}) by Mason (1975). These were used by some photoionization codes (e.g., Netzer's ION), while others (e.g., Ferland's CLOUDY) adopted the much smaller values of Ω. Recent computations for [Fe X] (Mohan et al. 1994, Pelan & Berrington 1995) and [Fe XIV] (Storey et al. 1996) seem to confirm the large effect of resonances, although large discrepancies are found between the two computations for [Fe X].

Acknowledgments. I would like to thank Alessandro Marconi for his continuous and competent help, and the organizing committee for the invitation.

References

Ashley, M. C. B., & Hyland, A. R. 1988, ApJ, 331, 532.

Bates, D. R., & Dalgarno, A. 1962, in Atomic Processes and Molecular Processes, ed. D. R. Bates (Academic Press: NY), p. 258.

[2] Editor's note: According to A. K. Pradhan, the values available from the Centre de Données Astronomiques de Strasbourg (CDS) are based on a more complete calculation and are the preferred values.

Butler, K., & Zeippen, C.J. 1994, A&AS, 108, 1.

Galavis, M.E., Mendoza, C., & Zeippen, C.J. 1995, A&AS, 111, 347.

Grandi, S.A. 1978, ApJ, 221, 501 (G78).

Graney, C.M., & Sarazin, C. 1990, ApJ, 364, 561 (GS90).

Herzberg, G. 1944, Atomic Spectra and Atomic Structure, (Dover Pub.: NY).

Kafatos, M., & Lynch, J.P. 1980, ApJS, 42, 611 (KL80).

Korista, K.T., & Ferland, G.J. 1989, ApJ, 343, 678.

Maiolino, R., et al. 1997, this volume.

Marconi, M., et al. 1996, A&A, in press (Ma96).

Marconi, M., et al. 1994, A&A, 291, 18 (M94).

Mendoza, C. 1983, in Planetary Nebulae, ed. D.R. Flower (Dordrecht: Reidel), 143.

Mason, H.E. 1975, MNRAS, 170, 651.

Mohan, M., Hibbert, A., & Kingston, A.E. 1994, ApJ, 434, 389.

Moorwood, A.F.M., Lutz, D., Oliva, E., Marconi, A., Netzer, H., Genzel, R., Sturm, E., & de Graauw, T. 1996, A&A, in press (Mo96).

Netzer, H., 1997, this volume.

Nussbaumer, H., & Osterbrock, D.E. 1970, ApJ, 161, 811.

Oliva, E., & Moorwood, A.F.M. 1990, ApJL, 348, L5.

Oliva, E., Salvati, M., Moorwood, A.F.M., & Marconi, A. 1994, A&A, 288, 457 (O94).

Oliva, E., Origlia, L., Kotilainen, J.K, & Moorwood, A.F.M. 1995, A&A, 301, 55.

Oliva, E., Pasquali, A., & Reconditi, M. 1996, A&A, 305, L21 (O96).

Osterbrock, D.E., Shaw, R.A., & Veilleux, S. 1990, ApJ, 352, 561.

Pelan, J., & Berrington, K.A. 1995, A&AS, 110, 209.

Penston, M.V., Fosbury, R.A.E., Boksenberg, A., Ward, M.J., & Wilson, A.S. 1984, MNRAS, 208, 347 (P84).

Reconditi, M., & Oliva, E. 1993, A&A, 274, 662.

Russel, S.C., & Dopita, M.A., 1990, ApJS, 74, 93.

Saraph, H.E., & Tully, J.A. 1994, A&AS, 107, 29 (ST94).

Saraph, H.E., & Storey, P.J. 1996, A&AS, 115, 151.

Seyfert, C.K. 1943, ApJ, 97, 28.

Storey, P.J., Mason, H.E., & Saraph, H.E. 1996, A&A, 309, 677.

Thompson, R.I. 1996, ApJL, 459, L61.

Viegas-Aldrovandi, S.M., & Contini, M. 1989, A&A, 215, 253 (VC89).

Zhang, H.L, Graziani, M., & Pradhan, A.K. 1994, A&A, 283, 319.